Battery anti-aging control for a plug-in hybrid electric vehicle with a hierarchical optimization energy management strategy

Bai, Y., He, H., Li, J., Li, S., Wang, Y. & Yang, Q.

Original citation & hyperlink:
Bai, Y, He, H, Li, J, Li, S, Wang, Y & Yang, Q 2019, 'Battery anti-aging control for a plug-in hybrid electric vehicle with a hierarchical optimization energy management strategy', Journal of Cleaner Production, vol. 237, 117841.
https://dx.doi.org/10.1016/j.jclepro.2019.117841

DOI 10.1016/j.jclepro.2019.117841
ISSN 0959-6526
ESSN 1879-1786

Publisher: Elsevier

Journal Pre-proof

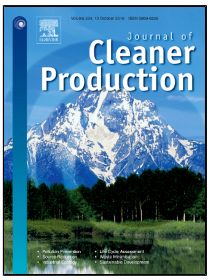

Battery anti-aging control for a plug-in hybrid electric vehicle with a hierarchical optimization energy management strategy

Yunfei Bai, Hongwen He, Jianwei Li, Shuangqi Li, Ya-xiong Wang, Qingqing Yang

PII:	S0959-6526(19)32707-6
DOI:	https://doi.org/10.1016/j.jclepro.2019.117841
Article Number:	117841
Reference:	JCLP 117841
To appear in:	*Journal of Cleaner Production*
Received Date:	15 April 2019
Accepted Date:	29 July 2019

Please cite this article as: Yunfei Bai, Hongwen He, Jianwei Li, Shuangqi Li, Ya-xiong Wang, Qingqing Yang, Battery anti-aging control for a plug-in hybrid electric vehicle with a hierarchical optimization energy management strategy, *Journal of Cleaner Production* (2019), https://doi.org/10.1016/j.jclepro.2019.117841

Word count: 7217.

Battery anti-aging control for a plug-in hybrid electric vehicle with a hierarchical optimization energy management strategy

Yunfei Bai[a], Hongwen He[a]*, Jianwei Li*[a], Shuangqi Li[a], Ya-xiong Wang[b], Qingqing Yang[c]

a. Beijing Institute of technology National Engineering Laboratory for Electric Vehicles, 100081 Beijing, China

b. School of Mechanical Engineering and Automation, Fuzhou University, Fuzhou, China

c. Faculty of Engineering, Environment and Computing, Coventry University, Coventry CV1 5FB, UK

** Corresponding authors: Hongwen He and Jianwei Li*

Abstract: This paper proposes a hierarchical optimization energy management strategy to suppress the battery aging in plug-in hybrid electric vehicles. In the first-level, a variable-threshold dynamic programming algorithm to distribute the power between the energy storage system and the engine is proposed. By adding supercapacitor to form the hybrid energy storage system, and using adaptive low-pass filtering algorithm, the power between the battery and the supercapacitor is distributed. To control the supercapacitor and battery to work within the capacity range, a power limits management module for redistributing the power between the engine, the supercapacitor and the battery is considered. The adaptive low-pass filtering algorithm and power limits management module constitute adaptive power allocation method in the second-level. After that, the rain-flow counting algorithm is applied in this paper to calculate battery aging cost. By using the rain-flow counting algorithm, the battery performances are analyzed, and the results show that the adaptive power allocation method can improve the battery service life by about 54.9% compared with the global dynamic programming algorithm. Considering the initial cost of the supercapacitor, the costs of battery aging, fuel consumption, electricity consumption, and management cost of retired batteries, compared with the global dynamic programming algorithm, the life cycle economy of the vehicle is improved by 12.4% under the proposed method.

Keywords: Plug-in hybrid electric vehicle; Hybrid energy storage system; Battery aging; Adaptive power distribution; Life cycle economy

Nomenclature:

CTF: cycles to failure	*PED: pure electric driving*
CTUDC: Chinese typical urban driving cycle	*PHEB: plug-in hybrid electric bus*
DOD: depth of discharge	*PHEV: plug-in hybrid electric vehicle*
DP: dynamic programming	*SOC: state of charge*
ESS: energy storage system	*SOE: state of energy*
ESU: energy storage unit	*TC: total cost*
HESS: hybrid energy storage system	*TM: traction motor*
ICE: internal combustion engine	*TOS: threshold of SOC*
ISG: integrated starter generator	*V-DP: variable-threshold dynamic programming*
OD: optimization driving	

1. Introduction:

As the energy shortage is becoming increasingly serious [1-4], there is an urgent need to find alternatives to conventional internal combustion engine (ICE) vehicles [5-7]. Due to longer driving range and excellent fuel economy [8-10], much attention has been focused on the development of plug-in hybrid electric vehicle (PHEV) which is equipped with a large capacity battery pack that can replenish power from the grid [11-13].

The configurations of PHEV power are divided into three categories, namely, the series configuration, the parallel configuration and the series-parallel configuration [14]. Among them, the series-parallel configuration is widely used because of various working modes. LiFePO4 is a positive active material for lithium-ion batteries and has been widely used in automotive applications [15-17]. Due to its characteristics including flat voltage plateau, high energy density, low toxicity and large safety range [18], the lithium-ion phosphate battery is widely used in electric vehicles and PHEVs. In this study, the energy storage system (ESS) of the target PHEB is built by the lithium-ion phosphate battery. Nevertheless, the cost of the lithium-ion battery is very high and the power density of the lithium-ion battery is low [19, 20]. The demand for instantaneous output and input power makes the lithium-ion battery frequently charge and discharge [21-23], which exacerbates battery aging, resulting in a severe capacity degradation in PHEV. Conversely, supercapacitor is characterized by high power density and high cycle-life [24-27], which could respond quickly to power demands [28-30]. The concept of the hybrid energy storage system (HESS), therefore, described by combining battery packs and supercapacitor groups [31], can effectively prolong the battery service life.

1.1 Literature review

Various methods have been proposed to allocate the output power between the battery and the engine. These previous energy control strategies only focus on improving fuel economy, among which the most extensively researched strategies are rule-based and optimization-based strategy [32-34]. Rule-based energy management strategies enable different driving modes by setting fixed thresholds. Lee et al [35] has introduced a rule-based strategy to distribute power between the battery and the engine for a PHEV, which ensures that the engine and the battery operate at high efficiency. However, the threshold setting depends on engineering experience. Optimization-based strategies can improve highly the performance of the power system for PHEVs [36-38]. With the development of intelligent algorithms, various optimization algorithms such as dynamic programming (DP) [39], particle swarm optimization (PSO)[40] [41] and fuzzy logic approach [42] have been developed, among which DP is the most widely used. Ref.[43] has described a method by applying DP realizing the optimal power allocation of PHEV, resulting in 20% improvement in fuel economy compared with traditional control strategy. Under the DP algorithm, the optimal fuel economy can be obtained, but the DP algorithm is a set of methods for solving the optimal strategy from the last step to the first step. As a result, the battery state of charge (SOC, which used to describe the amount of energy left in a battery compared with its full capacity) cannot be controlled, which may cause battery frequent cycling hence aggravates its aging. To ensure fuel economy while suppressing battery aging, a novel hierarchical optimization energy management strategy is proposed in this paper which can allocate the power between engine, battery and supercapacitor.

HESS is widely used in smoothing power fluctuations. Refs.[44-47] confirm that HESS with supercapacitor will greatly inhibit battery's aging. Some methods have been proposed to allocate the power between supercapacitor and battery inside HESS, such as rule-based control [48], fuzzy control

[49], optimal control based algorithm [50] and low-pass filtering algorithm [51, 52], among which the low-pass filtering algorithm is the most realistic. However, traditional first-order low-pass filtering algorithm can't monitor the remaining capacity of the battery and supercapacitor in real time, which can easily lead to over-charge and over-discharge of them. Moreover, the filter coefficient of the first-order low-pass filtering algorithm is fixed, which will cause the sub-high frequency signal not to be filtered and the large amplitude signal not to not followed well, resulting in a small reduction in the number of charge and discharge cycles of the battery. In order to reduce the number of battery charge and discharge cycles more and control the supercapacitor and the battery to work within the capacity range, a novel adaptive power allocation method is introduced in the paper which includes adaptive low-pass filtering algorithm and the power limits management module.

Currently, some studies have investigated the problem of battery aging in PHEV. Ref.[53] uses the neuro-fuzzy system to evaluate the health status of the power battery pack, clarifying the effects of battery charging and discharging depth, battery operating temperature and other factors on battery aging. In [54], the fuzzy logic method is used in battery modeling, and the influence of temperature on the parameters is described by fuzzy rules.

To estimate the service life of the battery, empirical model and data-driven model are proposed. Li et al [55] developed a cycle life model to predict the battery cycle-ability accurately. Ref.[56] has developed a lithium-ion battery temperature dependent model based on deep learning algorithm to estimate battery terminal voltage and SOC with low error. However, these methods are complicated in calculation process. In order to improve speed while maintaining accuracy, this paper proposes a simple but effective battery life model based on rain-flow counting algorithm.

1.2 Motivation and innovation

The demand for instantaneous output and input power exacerbates batteries aging. To ensure fuel economy while suppressing battery aging, the hierarchical optimization management strategy is designed. The key innovations of this paper are as follows:

1) To improve fuel economy while suppressing battery aging, a hierarchical optimization energy management strategy is proposed for a PHEV with multi-energy sources.
2) In the first level optimization, variable-threshold dynamic programming (V-DP) algorithm is developed to reduce the numbers of battery charge and discharge cycles.
3) In the second level optimization, adaptive power allocation algorithm is proposed to reduce battery charge and discharge frequency and rate.
4) A battery life model based on rain-flow counting algorithm is designed to optimize the hierarchical optimization energy management strategy and analyze the life cycle economy.

1.3 Organization of the paper

The rest of the paper is organized as follows: Section 2 briefly introduces PHEV configuration and builds ICE model, battery model, supercapacitor model, integrated starter generator (ISG) and traction motor (TM) model, and vehicle longitudinal dynamics model. Battery anti-aging control strategy with a hierarchical optimization approach is illustrated in section 3. Then, section 4 introduces life cycle economic analysis method based on rain-flow counting algorithm. In section 5, the results and discussion will be illustrated. Conclusions are drawn in section 6.

2. Plug-in hybrid electric vehicle modeling

2.1 PHEV configuration

A single-axis series-parallel PHEV is investigated in this paper, and its typical powertrain

configuration is shown in Fig. 1(a), which is consisted of a conventional internal combustion engine (ICE), an integrated starter generator (ISG), a traction motor (TM) and a battery pack. Compared with powertrain configuration a, powertrain configuration b adds a supercapacitor group shown in Fig.1(b), and other components are same in two configurations. Powertrain configuration a and b are the research object in this paper. The detailed parameters of the PHEV are listed in Table.1. The data-driven source comes from target PHEB, which is produced by Yutong Bus Company. The PHEB, that has been studied in [14, 57, 58], is 18 meters long and runs on city roads.

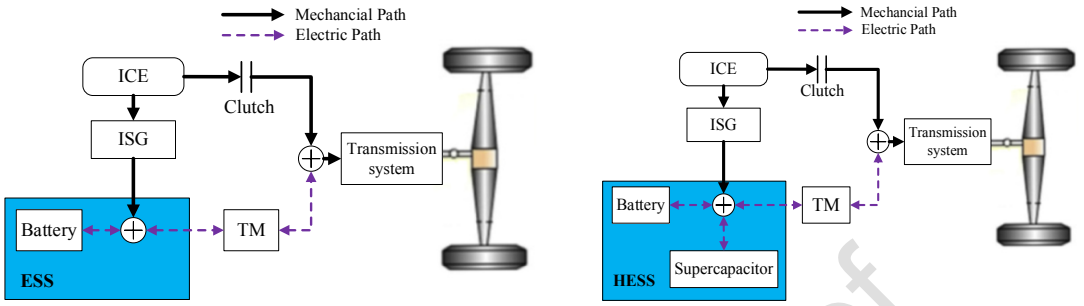

(a)The series-parallel powertrain with an ESS (b)The series-parallel powertrain with a HESS

Fig.1 Topology of different PHEV powertrains

Table.1 Specific parameters of the PHEV

Name	Parameters	Value	Parameters	Value
ICE	Maximum power/kW	147	Maximum torque/Nm	804
	Idle speed/rpm	650	Maximum speed/rpm	2600
ISG	Maximum power/kW	55	Maximum torque/N	500
TM	Maximum power/kW	168	Maximum torque/N	2000
Battery	Capacity/Ah	60	Voltage/V	576
Supercapacitor	Capacity/F	13.75	Voltage/V	576
Others	Vehicle loaded mass/kg	18000	Windward area/m^2	6.6
	Air resistance coefficient	0.55	Tire rolling radius/mm	473
	Rolling resistance coefficient	0.0095	Transmission efficiency	0.93

2.2 PHEV modeling

To provide the necessary simulation environment for the study of hierarchical optimization energy management strategy, the simulation model is built, including ICE model, battery model, supercapacitor model, TM model, ISG model and vehicle longitudinal dynamics model. The ICE model, the ISG model and the TM model are developed based on the experimental modeling method. The efficiency map of ICE, ISG and TM are expressed as the relationship between the speed and torque by a non-linear 3-D MAP from the experimental data. This modeling method is widely used [43, 59] and be proved with feasibility [60, 61]. The battery model, the supercapacitor model and the vehicle longitudinal dynamics model are based on mathematical modeling method.

2.2.1 ICE modeling

The ICE model together with the driving pattern provide the power requirements for the hybrid energy storage in this study. The key optimization is the power shared between the battery and the supercapacitor and the main contribution of the paper is the battery anti-aging control in the hybrid scheme. Therefore, the presented simulation is developed based on a MAP of the sets of ICE test data.

Note that BSFC is the abbreviation for brake specific fuel consumption. The ICE fuel consumption map is shown as Fig.2.

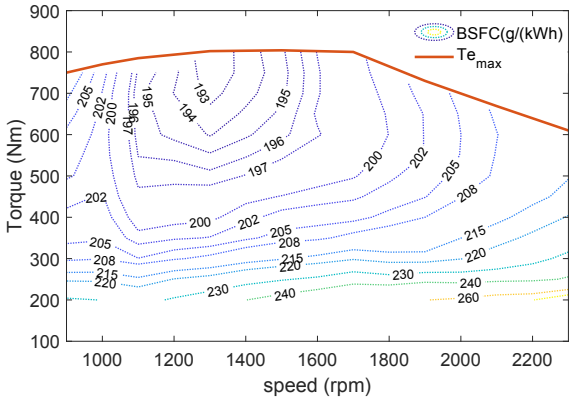

Fig.2 The ICE fuel consumption map [58]

2.2.2 Battery modeling

The study is developed based on the PHEB, in which the Lithium iron phosphate battery is used as the main power source. To analyze the dynamic characteristics of the lithium-ion battery, a simple but effective internal resistance battery model is built, and its charge state can be calculated by the following equation [62]:

$$\frac{dSOC}{dt} = -\frac{V_{OC} - \sqrt{V_{OC}^2 - 4 \cdot R_{\text{int}} \cdot P_B}}{2 \cdot R_{\text{int}} \cdot C} \tag{1}$$

Where, V_{oc} (V) is the battery open-circuit voltage; R_{int} (Ω) is the battery internal resistance; C (Ah) is the nominal capacity of the battery; P_B (W) is the electric power provided by the battery, which is determined by power requirements of the ISG and the TM.

2.2.3 Supercapacitor modeling

The dynamic characteristics of the supercapacitor group can be described as a series connection of a resistance R_C and an ideal capacitor, which can be described as follows [63]:

$$U_{ct} = U_{co} - R_c \cdot i_c \tag{2}$$

Where, U_{ct} (V) and U_{co} (V) are the output voltage and the ideal capacitor voltage respectively, and i_c (A) is the output current.

2.2.4 The ISG and TM modeling

The ISG and TM are both permanent magnet synchronous motor. The working efficiency η_m of the motor is an interpolation equation of the speed and torque, which is shown as follows [43]:

$$\eta_m(n_m, T_m) = f(n_m, T_m) \tag{3}$$

Where, n_m and T_m (Nm) are speed and torque of the motor, respectively.

Efficiency map of the ISG obtained from experimental data is shown in Fig.3 (a), and efficiency map of the TM obtained from experimental data is shown in Fig.3 (b).

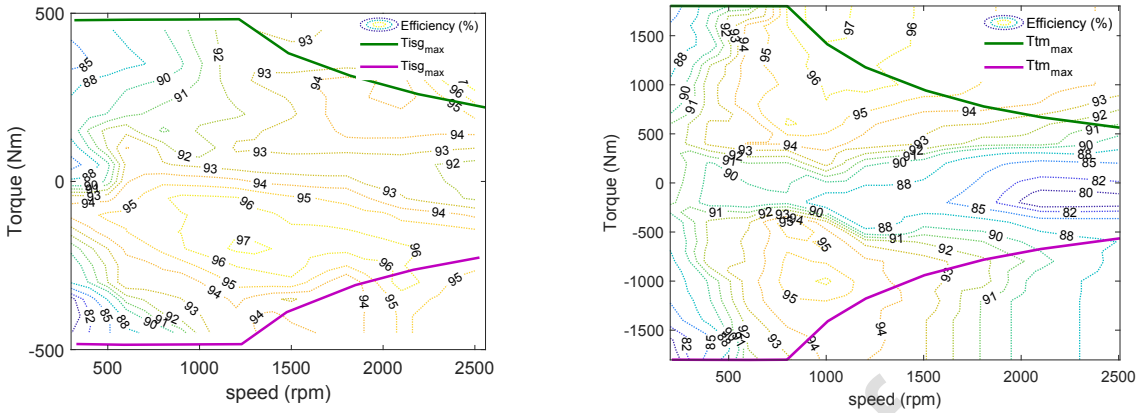

(a) Efficiency map of ISG (b) Efficiency map of TM

Fig.3 Efficiency map of the motor [62]

2.2.5 Vehicle longitudinal dynamics modeling

During the driving process, the driving force provided by the power system needs to overcome the driving resistance of the vehicle. In the longitudinal direction, the dynamic equation of the PHEV can be described as follows [58]:

$$F_d = F_w + F_f + F_i + F_a = \frac{1}{2} C_D A \rho v_r^2 + mgf\cos\alpha + mg\sin\alpha + \delta m\frac{dv}{dt} \tag{4}$$

Where: F_w (N), F_f (N), F_i (N), F_a (N) are aerodynamic drag, rolling resistance, climbing resistance and acceleration resistance, respectively. C_D is air resistance coefficient. A (m^2) is windward area. ρ (kg/m^3) is air density. V_r (m/s) is relative vehicle speed, which is relative to wind speed. m (kg) is the vehicle gross mass. g(m/s^2) is the gravitational acceleration. f is rolling resistance coefficient. α is the road gradient. δ is the mass factor that equivalently converts the rotational inertias of rotating components into translational mass (the value is 1.05). dv/dt (m/s^2) is driving acceleration.

3. Battery anti-aging control with a hierarchical optimization approach

Depth of discharge (DOD), number and rate of charge and discharge cycles will affect battery aging. To suppress battery life degradation, the hierarchical optimization energy management strategy is proposed in four levels, that the battery anti-aging control is shown in Fig.4.

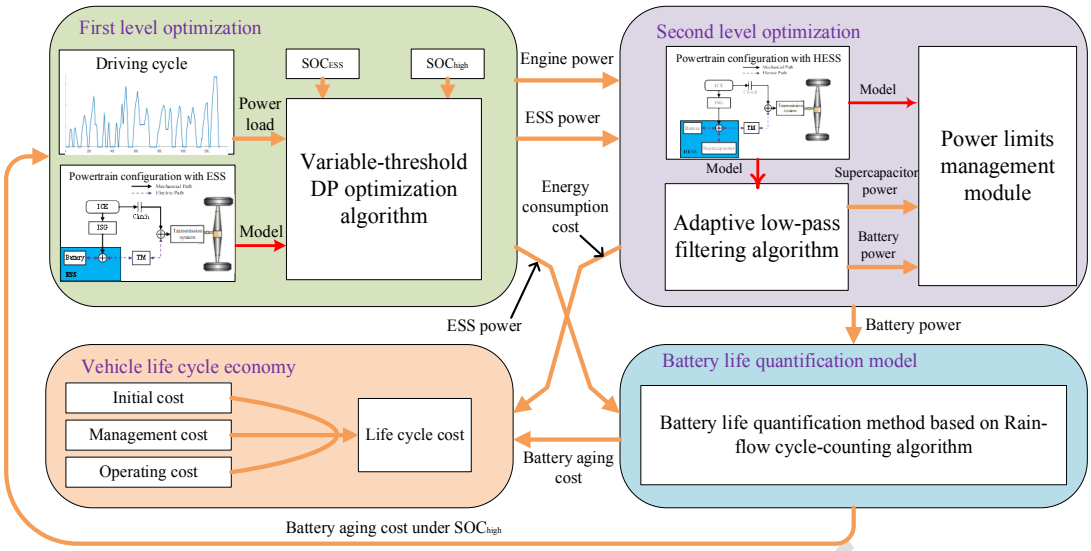

Fig.4 The battery anti-aging control frame

1) ***First-level optimization:*** Based on powertrain configuration with ESS, the V-DP algorithm is applied for each global driving condition discretizing the threshold of SOC of ESS within a certain range. When the SOC of ESS is above the threshold, the vehicle is in pure electric driving (PED), otherwise, the vehicle is in optimization driving (OD). For each threshold of SOC of ESS, firstly, ESS power and engine power through simulation based on V-DP is obtained. Then, battery aging cost based on battery life quantification model is set up with the calculation of fuel and electricity consumption costs based on ESS and engine powers. Finally, battery aging cost, fuel and electricity consumption costs to determine the optimal threshold is considered.
2) ***"Second-level optimization:*** Supercapacitor is introduced into the ESS forming the HESS. The power of ESS obtained in the first-level optimization is specified as the power of HESS in the Second-level optimization. The adaptive low-pass filtering algorithm is proposed to distribute the power between the battery and the supercapacitor inside the HESS. Then the power limits management module is used to control the supercapacitor and the battery working within the desired power range. The power limits management module is also functional to redistribute the power between the ICE and HESS when the power of the battery/SC HESS cannot meet the power requirement."
3) ***Battery life quantification model:*** In order to optimize the hierarchical optimization energy management strategy and analyze the life cycle economy of the vehicle, a simple but effective battery life quantification model based on rain-flow counting algorithm is proposed. The number of battery charge and discharge cycles can be obtained by the rain-flow counting algorithm. Hence, the aging cost of battery can be calculated based on the battery life model.
4) ***Vehicle life cycle economy:*** In order to evaluate the pros and cons of hierarchical optimization energy management strategy, the life cycle cost of the vehicle is analyzed. Since powertrain configuration a and powertrain configuration b have the same parameters except the energy storage unit (ESU), only the initial cost (supercapacitor group cost), operation costs (fuel and electricity consumption costs and battery aging cost) and management cost of retired batteries are quantified in this paper.

3.1 First-level optimization: variable-threshold dynamic programming (V-DP)

DP is a global optimization algorithm, which is mainly used to solve the optimization problem of

multi-stage decision making. The solution process of DP is based on the optimization principle proposed by Berman. The whole optimization process is decomposed into a series of single-step optimization sub-problems. The minimum cost function is obtained by the backward solution method, and finally the optimal decision sequence is obtained.

The whole vehicle can obtain the best fuel economy with the global optimal energy management based on DP algorithm. However, the DP strategy distributes the electric energy evenly in the running vehicles, which will cause frequent charging and discharging of the battery and accelerate battery aging. Therefore, V-DP algorithm is proposed discretizing the threshold of SOC in ESS within a certain range for each global driving condition as shown in Fig.5. When the SOC of ESS is above the threshold, the vehicle runs in PED, otherwise, the vehicle runs in OD. ESS power and engine power through simulation based on V-DP is obtained for each threshold of SOC in ESS, following with the battery aging cost acquisition based on battery life model and fuel and electricity consumption costs calculation based on ESS and engine powers. Finally, the optimal threshold can be determined by fuel consumption costs, electricity consumption costs and battery aging cost, that can be described as follows:

$$C_{total} = C_{init\_ESS} \times \eta + C_{fuel} + C_{elec} \tag{5}$$

Where, C_{init_ESS} is the initial cost of ESS; η is the battery life aging factor; C_{fuel} is fuel consumption cost; and C_{elec} is electricity consumption cost.

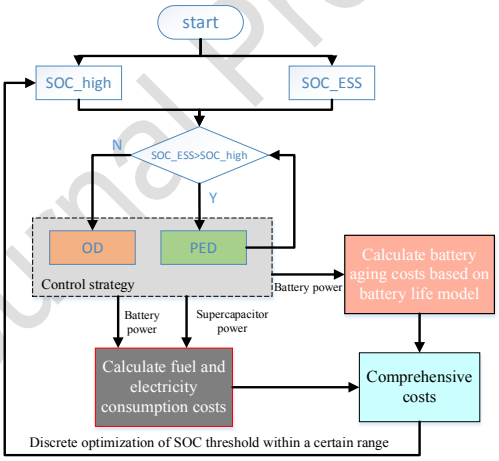

Fig.5 Variable-threshold DP algorithm

When the vehicle runs in PED, only the ESS is operated, the ICE and the ISG are always in the off state, and the clutch is always disengaged. Since the ESS is at a high SOC, the braking energy is not recovered.

When the vehicle in OD, the SOC of ESS is selected as system state variable. The ICE torque T_e, the ISG torque T_{ISG}, the TM torque T_m, the clutch state S_{clu}, and the braking torque T_b are the control variables for the system.

A plug-in hybrid system can be described as a nonlinear time-discrete system as shown in equation (6):

$$\begin{cases} x(t+1) = f(x(t), u(t)) \\ x(0) = x_0 \end{cases} \tag{6}$$

Where $x(t)$ is the SOC of battery at time t; $x(t+1)$ is the state at the *(t+1)*th time of the system; $u(t)$, namely T_e, T_{ISG}, T_m, S_{clu}, T_b, are the control quantities act on the vehicle at time *t*; f is the system state transfer function.

The establishment of the objective function of PHEV equivalent fuel consumption is shown in the following equation:

$$J = \sum_{k=0}^{N-1} L[x_k, u_k] \tag{7}$$

Where, $L[x_k, u_k]$ is the equivalent fuel consumption which includes fuel and electricity consumption cost at time *k*. *J* is the total equivalent fuel consumption.

To ensure stable operation of the ICE, ISG, TM and battery, the following constraints are established in equation (8):

$$\begin{cases} SOC_{\min} \le SOC_k \le SOC_{\max} \\ n_{e\_\min} \le n_{e\_k} \le n_{e\_\max} \\ T_{e\_\min}(n_{e\_k}) \le T_{e\_k} \le T_{e\_\max}(n_{e\_k}) \\ n_{ISG\_\min} \le n_{ISG\_k} \le n_{ISG\_\max} \\ T_{ISG\_\min}(n_{ISG\_k}, SOC_k) \le T_{ISG\_k} \le T_{ISG\_\max}(n_{ISG\_k}, SOC_k) \\ n_{m\_\min} \le n_{m\_k} \le n_{m\_\max} \\ T_{m\_\min}(n_{m\_k}, SOC_k) \le T_{m\_k} \le T_{m\_\max}(n_{m\_k}, SOC_k) \\ T_{d\_k} = T_{e\_k} + T_{ISG\_k} + T_{m\_k} + T_{b\_k} / i_0 \\ n_{m\_k} = n_{e\_k} = n_{ISG\_k} \quad if \quad S_{clu} = 1 \\ n_{e\_k} = n_{ISG\_k} \quad if \quad S_{clu} = 0 \\ T_{e\_k} + T_{ISG\_k} = 0 \quad if \quad S_{clu} = 0 \end{cases} \tag{8}$$

Where, n_{e_k} (rpm) and T_{e_k} (Nm) are the speed and output torque of the engine at the k^{th} step, respectively; n_{ISG_k} (rpm) and T_{ISG_k} (Nm) are the speed and output torque of the ISG at the k^{th} step, respectively; n_{m_k} (rpm) and T_{m_k} (Nm) are the speed and output torque of the TM at the k^{th} step, respectively; T_{b_k} (Nm) is the hydraulic brake torque at the k^{th} step; and the subscripts min and max in the variables denote the maximum and minimum of those variables, respectively.

3.2 Second-level optimization: Adaptive power allocation method

The power is distributed between ESS and ICE considering the battery aging cost, fuel and

electricity consumption costs in the first-level optimization. In order to suppress the battery aging further, supercapacitor is added in ESS to form the HESS. An adaptive power allocation method is pointed out to redistribute the power between ICE, battery and supercapacitor as shown in Fig.6, which is mainly composed of two parts: adaptive low-pass filtering algorithm and power limits management module. The power of HESS between the battery and the supercapacitor, which is assigned to the power of ESS obtained in the first-level optimization, is distributed by using the adaptive low-pass filtering algorithm proposed in this paper. In order to control the operation of supercapacitor and batteries in the capacitor range, the power limits management module redistributes power between ICE, supercapacitor and battery.

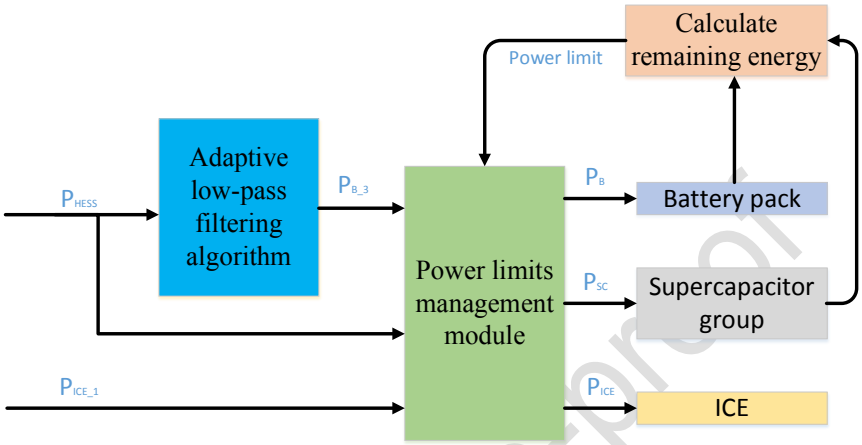

Fig.6 Adaptive power distribution method

3.2.1 Adaptive low-pass filtering algorithm

The first-order low-pass filtering algorithm can quickly distribute the power between battery and supercapacitor inside HESS, after which, the battery power output is smoothed and the number of charge and discharge cycles of battery is greatly reduced. However, the filter coefficient of the first-order low-pass filtering algorithm is fixed, which will cause the sub-high frequency signal to not be filtered and the large amplitude signal to not be followed well, resulting in a small reduction in the number of charge and discharge cycles of the battery. Moreover, due to the large difference, the size of the supercapacitor group is large, which is not conducive to the installation inside the vehicle.

To solve these issues, an adaptive low-pass filtering algorithm is used. The battery power $P_B(t)$ and supercapacitor power $P_{SC}(t)$ at time t can be obtained by the following equations:

$$P_B(t) = (1 - k(t)) \times P_B(t-1) + k(t) \times P_{HESS}(t) \tag{9}$$

$$P_{SC}(t) = P_{HESS}(t) - P_B(t) \tag{10}$$

Where, $k(t)$ is the filter coefficient. The smaller the filter coefficient is, the smoother the filter results are, but the lower the sensitivity is.

The power signal of ESS obtained by the first-level optimization can be divided into three modes:

Mode 1: Power data changes rapidly in a certain direction.

Mode 2: Power data oscillates rapidly within a certain range.

Mode 3: Power data changes slowly and the oscillation frequency is low.

The adaptive low-pass filtering algorithm shown in Fig.7 is able to accurately identify the three modes and give the corresponding dynamic filter coefficients. In mode 1, it is necessary to dynamically increase the filter coefficient, which can follow the change of the original data in the trend, so that the peak power of the supercapacitor is not too high, meanwhile the size of the supercapacitor group will be reduced. In mode 2, a small filter coefficient is given, which can filter out the high-frequency power signal, greatly reduce the number of charge and discharge cycles of the battery. In mode 3, a suitable filter coefficient is given to achieve the effect of first-order low-pass filtering.

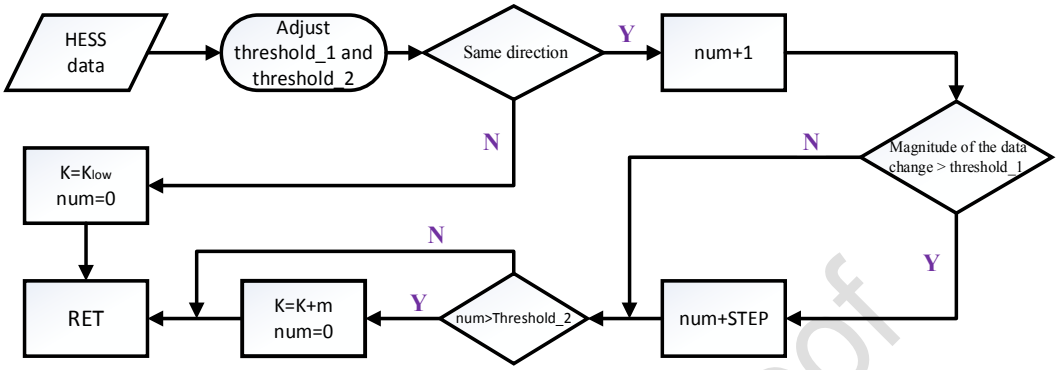

Fig.7 Adaptive low-pass filtering algorithm

3.2.2 Power limits management module

Since the charge and discharge power of the battery and supercapacitor, which are easy to be overcharged and over-discharged, are not limited, so the robustness of the entire control strategy will become weak. Aiming at this issue, a novel power limits management module is shown in Fig.8, which can achieve two functions. One is that limiting the maximum or minimum power output of the battery and supercapacitor based on the state of energy (SOE) derived in Eq.11. Another is that power limits management module is performed to minimize the tracking error of the charging and discharging power of the HESS when the battery or supercapacitor has insufficient capacity.

$$SOE_{ESU} = 1 - \frac{\int_0^t P_{ESU}\,dt}{E_{ESU}} \tag{11}$$

Limit module 1 and 3 in all three limit modules can limit battery power, and supercapacitor power is limited by limit module 2. The operation steps of the power limits management module are as follows:

Step 1: The battery power P_{B_3} is obtained by the adaptive low-pass filtering passes through the limit module 1 to get P_{B_2}, which ensure the battery operates within the capability range.

Step 2: By the difference between power of HESS P_{HESS} and P_{B_1}, the supercapacitor power P_{SC_1} can be obtained.

Step 3: P_{SC_1} pass through limit module 2 to obtain P_{SC}, which ensure the supercapacitor operates within the capability range.

Step 4: The difference between P_{SC_1} and P_{SC} results in tracking error of the charging and discharging power of the battery. P_{B_1} passes through the module 3 to get P_B.

Step 5: If the sum of battery power P_B and supercapacitor power P_{SC} cannot meet the HESS requirements, the power between HESS and ICE will be distributed. Finally, the battery power P_B, the supercapacitor power P_{SC} and ICE power P_{ICE} are obtained.

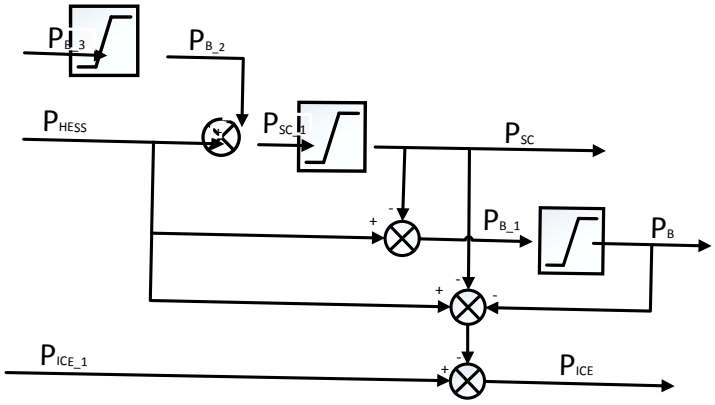

Fig.8 Power limits management module frame

To ensure the battery and supercapacitor operation within the capability range, the corresponding control strategies for the three limit modules is developed. Limit module 1 and 3 have the same control rules to define E_{B_r} as battery residual energy, $E_{B\_\max}$ as the maximum energy setting of the battery, P_{B_1} as the battery power input to the limit module, P_B as the battery power output from the limit module, and P_{K-1} as the battery power at the last moment. Control strategy is formulated to minimize the number of charge and discharge cycles of the battery. Limit model 3 is implemented with the following rules (limit model 1 is same with limit model 3).

If $E_{B\_r} > E_{B\_\max}$ & $P_{B\_1} > 0$, then $P_B = P_{B\_1}$;

If $E_{B\_r} > E_{B\_\max}$ & $P_{B\_1} < 0$ & $P_{K-1} < 0$, then $P_B = 0$;

If $E_{B\_r} > E_{B\_\max}$ & $P_{B\_1} > 0$ & $P_{K-1} > 0$, then $P_B = P_{K-1}$;

If $E_{B\_\min} < E_{B\_r} < E_{B\_\max}$, then $P_B = P_{B\_1}$;

If $E_{B\_r} < E_{B\_\max}$ & $P_{B\_1} < 0$, then $P_B = P_{B\_1}$;

If $E_{B\_r} < E_{B\_\max}$ & $P_{B\_1} > 0$ & $P_{K-1} < 0$, then $P_B = P_{K-1}$;

If $E_{B\_r} < E_{B\_\max}$ & $P_{B\_1} < 0$ & $P_{K-1} > 0$, then $P_B = 0$;

Limit module 2 limit the supercapacitor power that E_{C_r} is supercapacitor residual energy, $E_{C\_\max}$ is the maximum power setting of the supercapacitor, P_{SC_1} is the supercapacitor power input to the limit module, and P_{SC} is the supercapacitor power output from the limit module. Owing to high cycle-life, the smoothness of the power curve of the supercapacitor is not in consideration. Limit model 2 is implemented with the following rules.

If $E_{SC\_r} > E_{SC\_\max}$ & $P_{SC\_1} > 0$, then $P_{SC} = P_{SC\_1}$;

If $E_{SC\_r} > E_{SC\_\max}$ & $P_{SC\_1} < 0$, then $P_{SC} = 0$;

If $E_{SC\_\min} < E_{SC\_r} < E_{SC\_\max}$, then $P_{SC} = P_{SC\_1}$;

If $E_{SC\_r} < E_{SC\_\max}$ & $P_{SC\_1} > 0$, then $P_{SC} = 0$;

If $E_{SC\_r} < E_{SC\_\max}$ & $P_{SC\_1} < 0$, then $P_{SC} = P_{SC\_1}$;

4. Life cycle economic analysis based on rain-flow counting algorithm

4.1 Battery life quantification model

The battery life quantification model is established by the combination of cycles to failure chart and the rain-flow counting algorithm. This modeling method has proven to be efficient and accurate [44, 55].

4.1.1 Rain-flow counting algorithm

The rain-flow counting algorithm was first used in the fatigue life analysis of metals, which can record the number of cycles and the corresponding amplitude.

The rain-flow counting algorithm is operated as follows [64]:

1) The rain flow sequentially flows from the inside of the peak position of the load time history down the slope.
2) The rain begins to flow from a peak point and stops flowing when it encounters a peak larger than its starting peak.
3) When the rainwater encounters the rain flowing down, it must stop flowing.
4) The amplitude of each loop is taken down by getting rid of the full loops.

4.1.2 Battery life modeling

The life of the battery is affected by the number and depth of charge and discharge cycles. The more frequent the battery is charged or discharged, the greater depth of charge and discharge is, the shorter service life of the battery is. The rain-flow counting algorithm is used to record the number of charge and discharge cycles and the corresponding DOD of the battery.

For a uniform batch of batteries, the battery manufacturer gives a set of life data, that is, the relationship between cycles to failure (CTF) and the DOD of the battery at a certain discharge speed, as shown in the Fig.9. Using power function to fit this set of data, the F_{CD} equation is shown in Eq.12. After curve fitting, the coefficient in the above formula can be obtained: $a = 1075.1, c = -1.027$.

$$CTF = F_{CD}(DOD) = a \cdot DOD^{c} \tag{12}$$

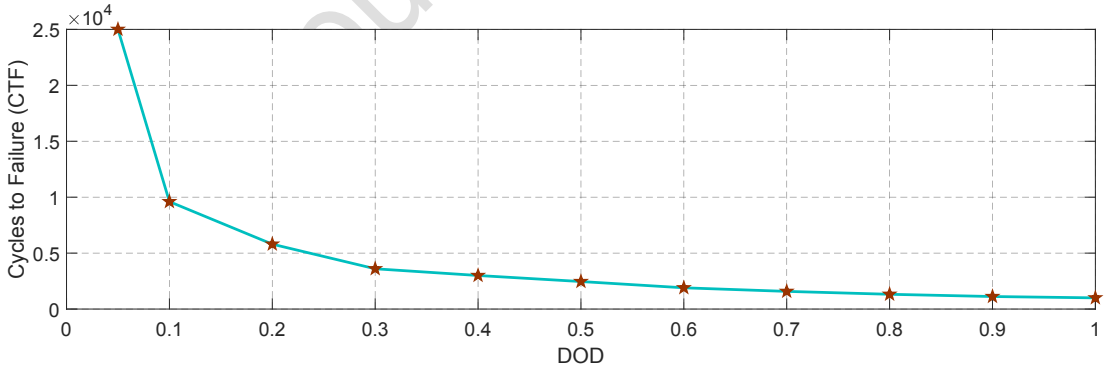

Fig.9 Cycles to failure vs. depth of discharge

The relationship between the battery life aging factor η, which is affected by the number of battery cycles and the corresponding DOD can be described as follows:

$$\eta = 1/CTF \tag{13}$$

According to the global cycle numbers obtained by the rain-flow counting algorithm and the corresponding DOD data, the total battery aging can be calculated by Eq.14.

$$D = \sum_{i=1}^{i=n} \eta_i \tag{14}$$

Thereby the quantified life of the battery can be obtained by Eq.15.

$$L_B = T/D \tag{15}$$

Battery life quantification flow chart is shown in Fig.10.

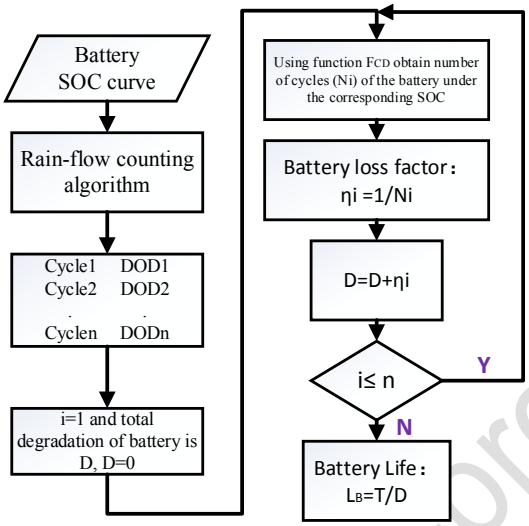

Fig.10 Battery life quantification model

4.2 Life cycle economy

This paper mainly carried out life cycle cost analysis for powertrain configuration a and powertrain configuration b. The difference between these two configurations is that configuration a loads ESS and configuration b loads HESS. Therefore, the cost of ESU, costs of fuel consumption and electricity consumption, and management cost of retired batteries will take into account when analyzing the life cycle cost of the vehicle.

4.2.1 Initial cost

Initial cost mainly includes the cost of ESU loaded on the vehicle. As for configuration a, the initial cost is the battery pack displayed below:

$$C_{B\_init} = \rho_B \times E_B \tag{16}$$

$$E_B = Q_B \cdot U_B / 1000 \tag{17}$$

Where: ρ_B and E_B are the price ($/kWh) and energy (kWh) of battery, respectively. Q_B and U_B are capacity (Ah) and voltage (V) of the battery, respectively.

As for configuration b, the initial cost is the total market price of the battery pack and the supercapacitor group loaded by the vehicle:

$$C_{SC\_init} = \rho_{SC} \times E_{SC} \tag{18}$$

$$E_{SC} = C_{SC} \cdot U_{SC}^2 / (2 \times 1000 \times 3600) \tag{19}$$

$$C_{HESS\_init} = C_{B\_init} + C_{SC\_init} \tag{20}$$

Where: ρ_{SC} and E_{SC} are the price ($ per kWh) and energy (kWh) of supercapacitor, respectively. C_{SC} and U_{SC} are capacity (F) and voltage (V) of the supercapacitor, respectively.

4.2.2 Operating costs

Due to the high cycle life of the supercapacitor, there is no need to replace it during the entire life cycle of the vehicle. Therefore, operating costs mainly include fuel consumption cost, electricity consumption cost and battery aging cost throughout the life cycle, as described below:

$$C_{oper} = C_{fuel\_N} + C_{elec\_N} + C_{B\_aging} \tag{21}$$

$$\begin{cases} C_{fuel\_N} = N \times 300 \times V_e \times \rho_{fuel} \\ C_{elec\_N} = N \times 300 \times E_B \times \rho_{elec} \\ C_{B\_aging} = C_{B\_init} \times \eta \times N \end{cases} \tag{22}$$

Where N is the life cycle of the whole life, V_e (liter) is the engine fuel consumption per day; ρ_{fuel} ($ per liter) is the price of diesel; ρ_{elec} ($ per kWh) is the price of electric.

4.2.3 Management cost of retired batteries

Aging lithium-ion batteries are processed through landfill routes. Hence the aging batteries management cost can be described below:

$$C_{mana} = N_{rep} \times M_B \times \rho_{rep} \tag{23}$$

Where N_{rep} is the number of replacements during the life cycle, M_B (kg) is the total mass of the car battery pack, ρ_{rep} ($ per replacement) is the management cost of one replacement. Based on the proposed retired batteries cost function, the management cost of the retired batteries will be added in the Section 5.3 “Life cycle cost analysis”.

4.2.4 The total cost of the life cycle

This paper calculates the battery aging cost after each driving based on the battery life model. Therefore, the initial cost only includes the initial cost of the supercapacitor shown as Eq.20, and the initial and replacement costs of the battery pack are all integrated into the operating costs.

$$C_{init} = C_{SC\_init} \tag{24}$$

The total costs include initial cost, operating costs, and the management of aged batteries, as described below:

$$C = C_{init} + C_{oper} + C_{mana} \tag{25}$$

5.Results and discussion

All the models including PHEV model and battery life quantification model are established in Matlab/Simulink as a platform. The simulation is completed using a computer with an Intel Core i7-8550U 1.99 GHz processor, 8 GB of RAM and 64-bit Windows operating system. The main object is a PHEB driving in city condition. In the simulation process, the Chinese typical urban driving cycle (CTUDC) is selected as shown in Fig.11, and the specific indicator parameters of CTUDC are shown in Table.3. The vehicle model is in operation continuously for twelve CTUDCs to verify the pros and cons of the control strategy. The price of battery is 300 $ per kWh (according to Ref.[60]), the energy of battery pack is 34.56 kWh calculated by Eq.16, so the initial cost of battery packs is 10368 $ calculated by Eq.15. The price of supercapacitor is 3600 $ per kWh (according to Ref.[65]), the energy of supercapacitor group is 0.63 kWh calculated by Eq.18, so the initial cost of supercapacitor group is 2268 $ calculated by Eq.17. The price of diesel is 1.04 $ per liter, and electric price is 0.18 $ per kWh (according to data on 02 Feb 2019 in Beijing).

Table.3 CTUDC indicator parameter table

Parameters	Value	Parameters	Value
Average speed/(km/h)	16.2	Percentage of time spent on idle/%	29.0
Maximum speed/(km/h)	60.0	Percentage of time taken at a constant speed/%	17.0
Total mileage/km	5.8	Acceleration time percentage/%	32.0
Total driving time/s	1314	Percentage of time spent decelerating/%	22.0

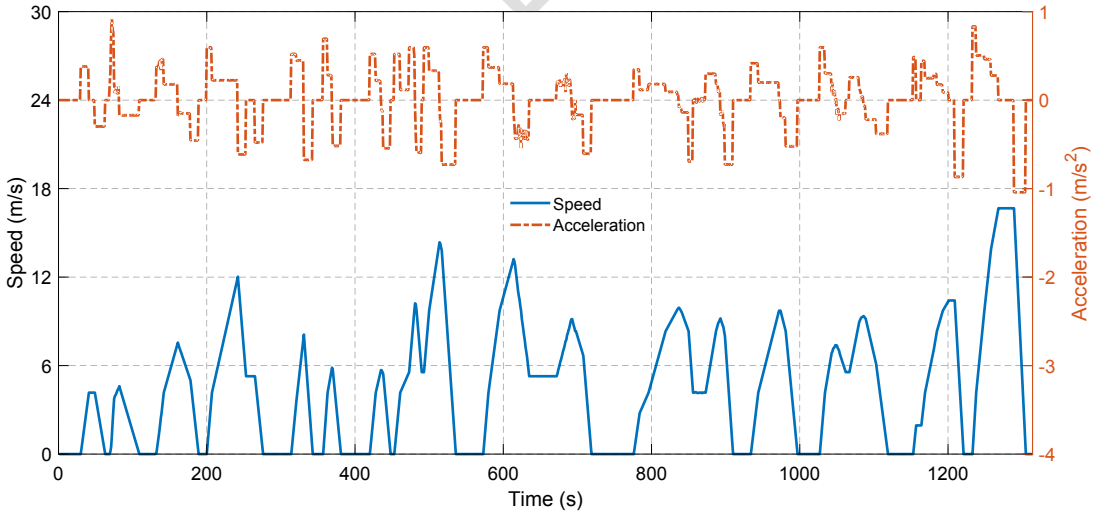

Fig.11 The velocity and acceleration of CTUDC driving cycle

5.1 V-DP algorithm verification

To suppress battery aging, V-DP algorithm is proposed to distribute the power between ESS and ICE. Considering the electricity and fuel consumption costs, and battery aging cost under the overall conditions, the optimal threshold is selected.

The threshold of the SOC of the ESS is discretized between 0.9 and 0.5, and each discrete point data is brought into the V-DP algorithm. The results are shown in Fig.12 and Fig.13.

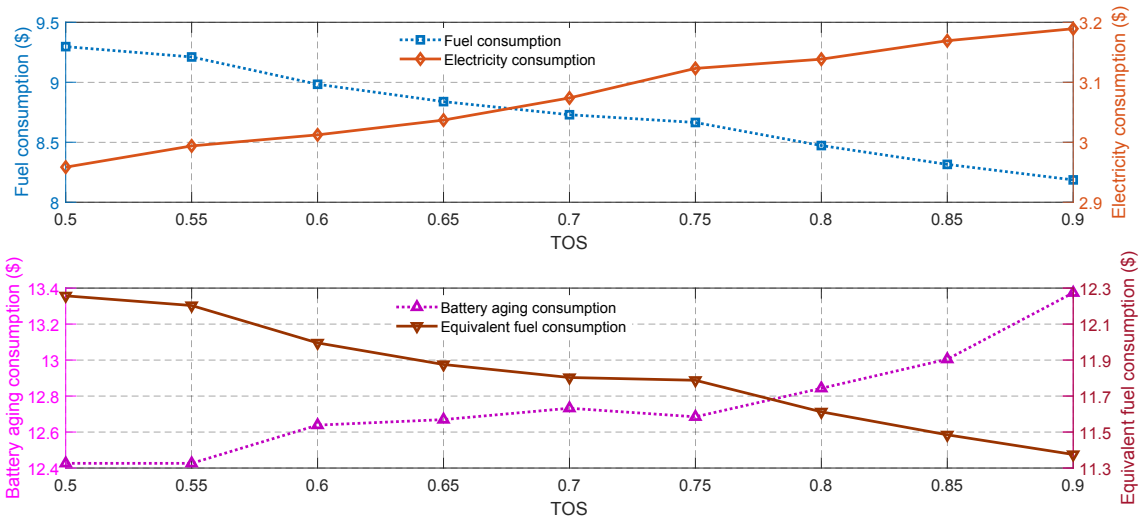

Fig.12 Energy consumption costs and battery aging cost at various thresholds

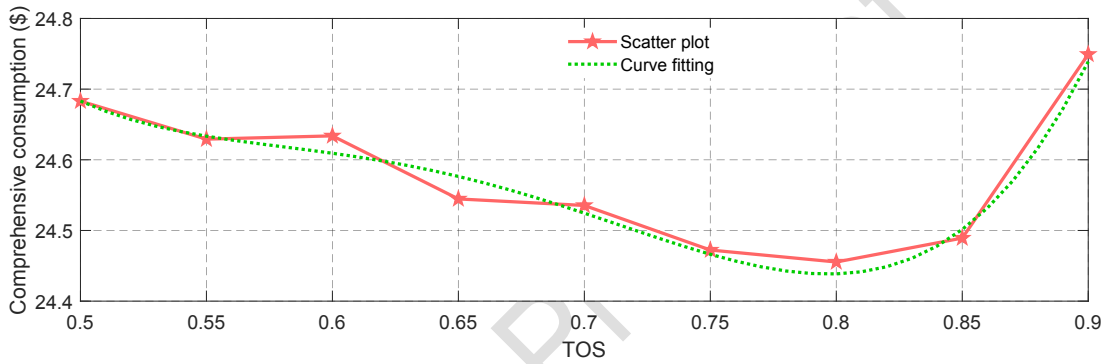

Fig.13 Total cost at various thresholds

As shown in Fig.12, the fuel consumption cost gradually decreases with the threshold increasing, but the electricity consumption cost and the sum of fuel and electricity consumption cost gradually increases. This proves that the vehicle equivalent fuel economy is optimal under the global DP. However, as the threshold decreases, the aging cost of the battery tends to decrease gradually.

As shown in Fig.13, by considering the costs of fuel consumption, electricity consumption and battery aging, the total cost (TC) decreases first and then slowly increases as the threshold decreases. Using Chebyshev polynomials to fit the data of the total cost is shown as follows (Note that TOS is the abbreviation for threshold of SOC):

$$TC = b_0 \cdot TOS^4 + b_1 \cdot TOS^3 + b_2 \cdot TOS^2 + b_3 \cdot TOS + b_4 \tag{26}$$

After curve fitting, the coefficient in the above formula can be obtained: $b_0 = 157.29$, $b_1 = -407.32$, $b_2 = 391.31$, $b_3 = -166.06$, $b_5 = 50.97$. Based on the Eq.26, when TOS is 0.8, the TC is minimum. Compared to the global DP algorithm, the overall cost is reduced by 2.2%. Record V-DP with a threshold of 0.8 as V0.8-DP.

As shown in Fig.14, the number and depth of battery charge and discharge cycles can be obtained through the rain-flow counting algorithm. For different thresholds, the SOE of the battery always drops from 0.9 to 0.2 under global conditions. Therefore, only the small loops in the SOE change process are compared and analyzed. As shown in Fig.14, as the threshold decreases, the total number

of battery charge and discharge cycles gradually decreases. The number of charge and discharge cycles of the battery under global DP is 254. When the threshold is 0.8, it drops to 244, and when the threshold is 0.5, it drops to 236. The maximum value of the y coordinate is gradually decreased because the time of the vehicle in PED gradually increases as the threshold decreases. This causes the number of charge and discharge cycles of the battery dropping sharply at a high SOE value, and effectively suppressing aging of the battery.

The dynamic programming algorithm is used as the benchmark for comparison. The battery life is 776 days based on the DP and battery life model. In the first-level optimization, the battery life is 809 days based on the V0.8-DP and battery life model. Therefore, comparing with global DP, the first level of optimization is able to improve the battery lifetime by 4.25%.

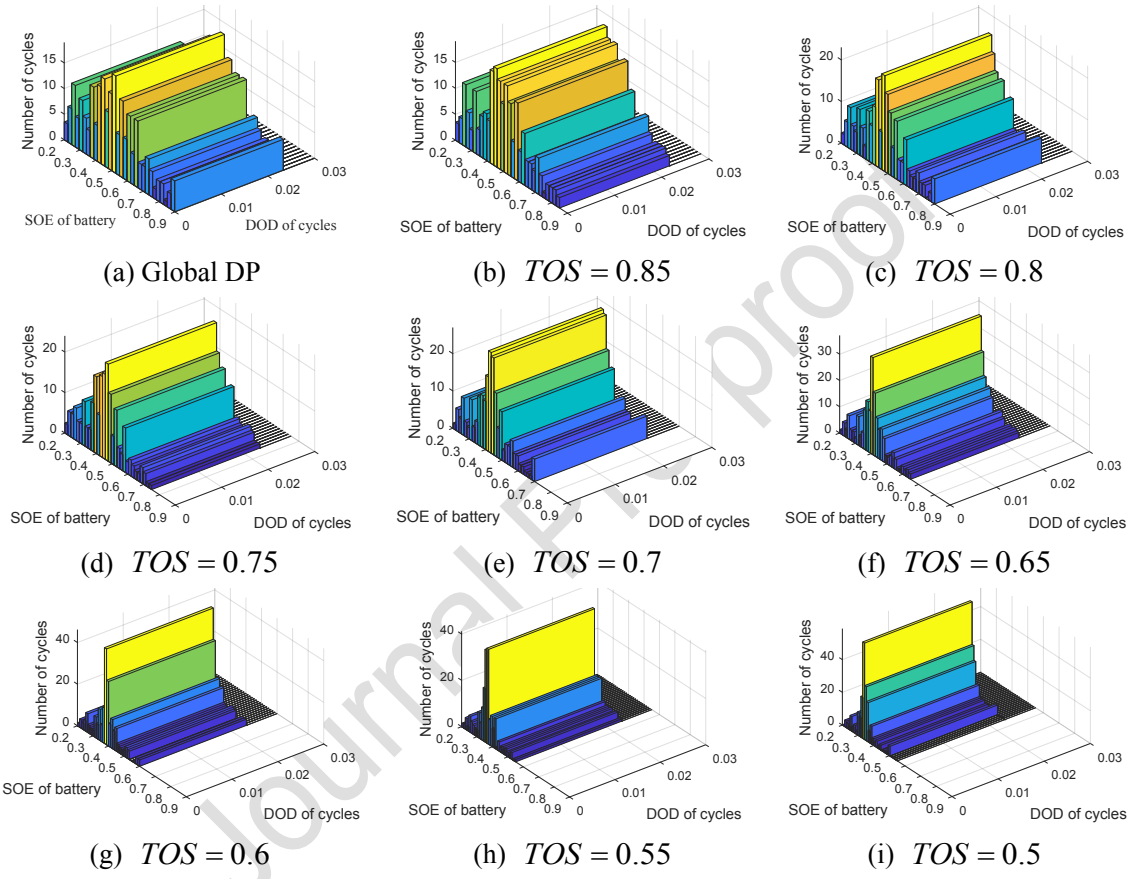

(a) Global DP (b) $TOS = 0.85$ (c) $TOS = 0.8$

(d) $TOS = 0.75$ (e) $TOS = 0.7$ (f) $TOS = 0.65$

(g) $TOS = 0.6$ (h) $TOS = 0.55$ (i) $TOS = 0.5$

Fig.14 Number and depth of battery charge cycles and discharge at various thresholds

As shown in Fig.15, the fuel and electricity costs are compared under global DP and V0.8-DP condition. The fuel consumption cost of V0.8-DP is lower than the global DP, but the electricity consumption cost of V0.8-DP is higher than the global DP at the beginning. As simulation time increases, the fuel consumption of V0.8-DP is gradually higher than the global DP, and the electricity consumption of V0.8-DP is gradually lower than global DP. The reason is that vehicle runs long in PED based on V0.8-DP with no engine working at this stage. However, with the simulation time increases, the SOC of the battery quickly drops to 0.8, the engine starts to work, fuel consumption cost begins to increase, and electricity consumption cost gradually decreases.

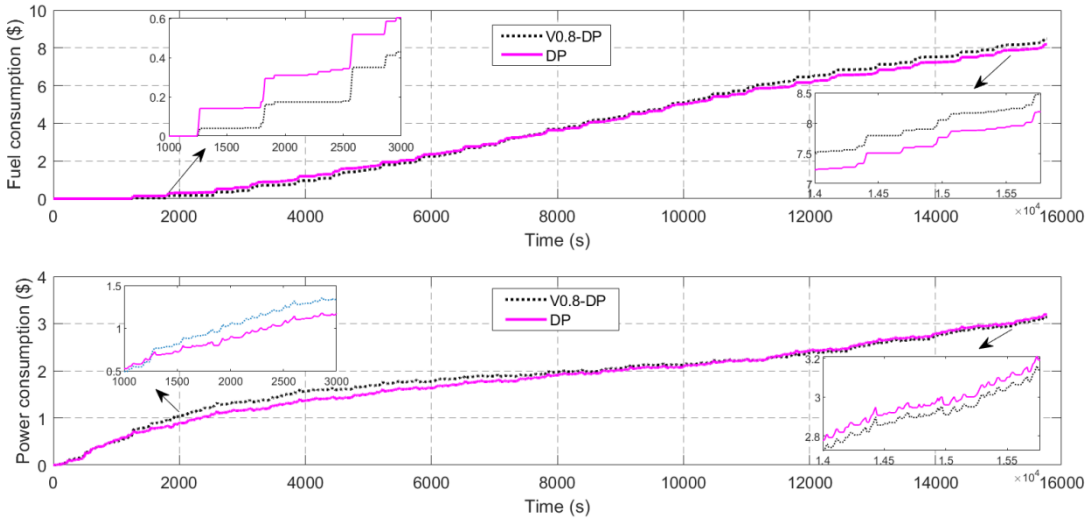

Fig.15 Comparison of energy consumption under two algorithms

5.2 Adaptive power allocation verification

5.2.1 Adaptive low-pass filtering verification

Supercapacitor is equipped in ESS to form the HESS to further inhibit battery aging. The power of ESS obtained in first-level optimization is specified as the power of HESS, and adaptive low-pass filtering algorithm is used to distribute the power between battery and supercapacitor in HESS. The ICE and ESS in powertrain configuration a have been allocated via the V0.8-DP. As shown in Fig.16, the battery power obtained by adaptive low-pass filtering is much smoother, which means that the rate of battery charge and discharge is reduced a lot, and battery aging is suppressed to a great extent.

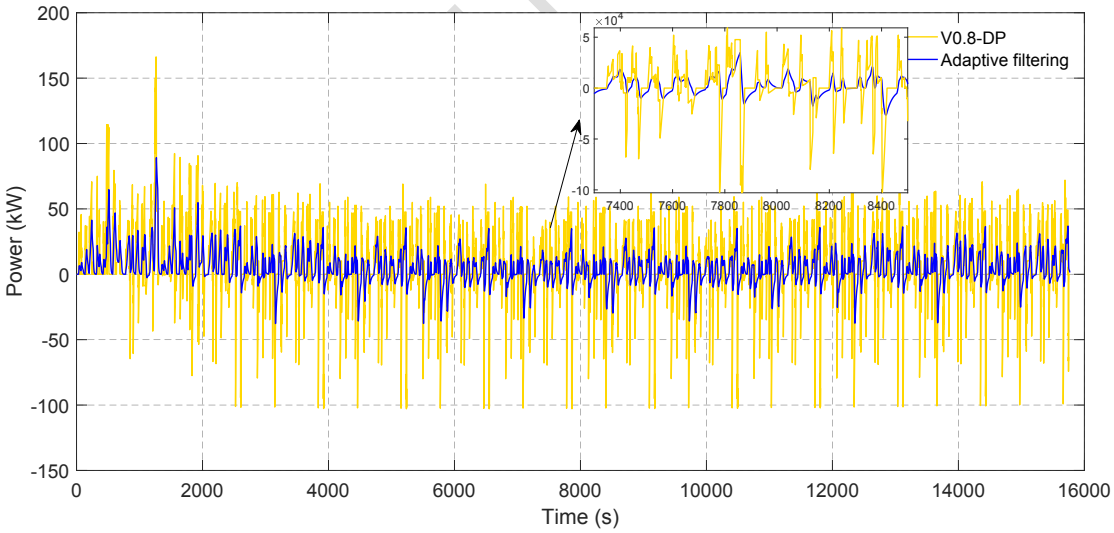

Fig.16 Comparison of battery power before and after adaptive filtering

As shown in Fig.17, the SOC curve of the battery after adaptive low-pass filtering is significantly smoother. The amplitude and number of battery charge and discharge cycles are significantly reduced, which will effectively inhibit battery aging.

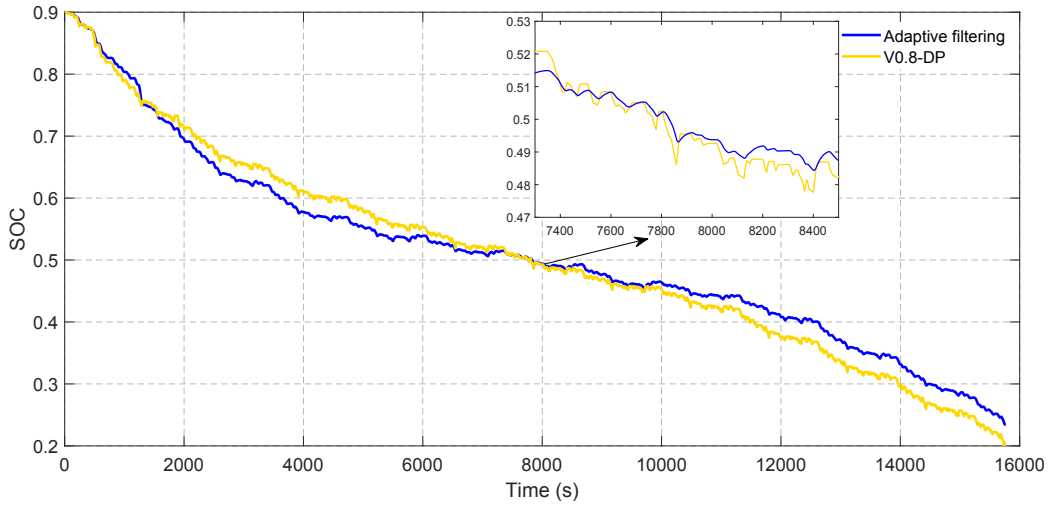

Fig.17 Battery SOC comparison before and after adaptive filtering

5.2.2 Power limits management module verification

Adaptive power allocation method is able to inhibit battery aging effectively. However, the battery and the supercapacitor over-charge and over-discharge problems are prone to occur because the adaptive low-pass filtering method cannot monitor the remaining energy of them. The result obtained by adaptive power allocation method is shown in Fig.18, the supercapacitor has a serious over-discharge problem because of low energy density, which greatly reduce the stability of the vehicle's power.

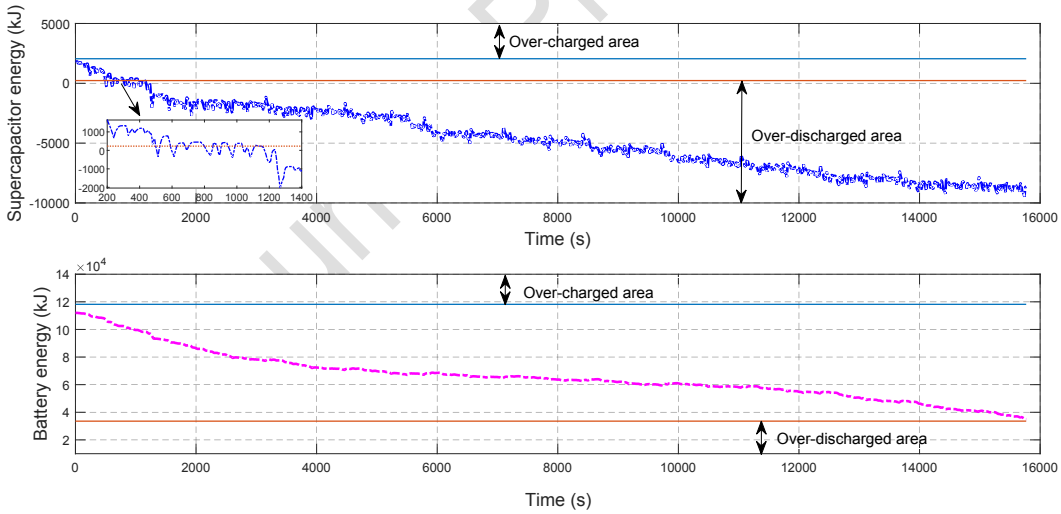

Fig.18 The remaining energy of the battery and the supercapacitor is obtained by adaptive power allocation

To control the supercapacitor and the battery working within the capacity range, power limits management module is proposed to redistribute the power between engine, supercapacitor and battery. The result obtained by power limits management module is shown in Fig.19, both the supercapacitor and the battery work within the set energy range, and power limits management module is real-time. Therefore, under any working conditions, the supercapacitor and the battery will not have the problem of over-charging and over-discharging no matter how long the driving time.

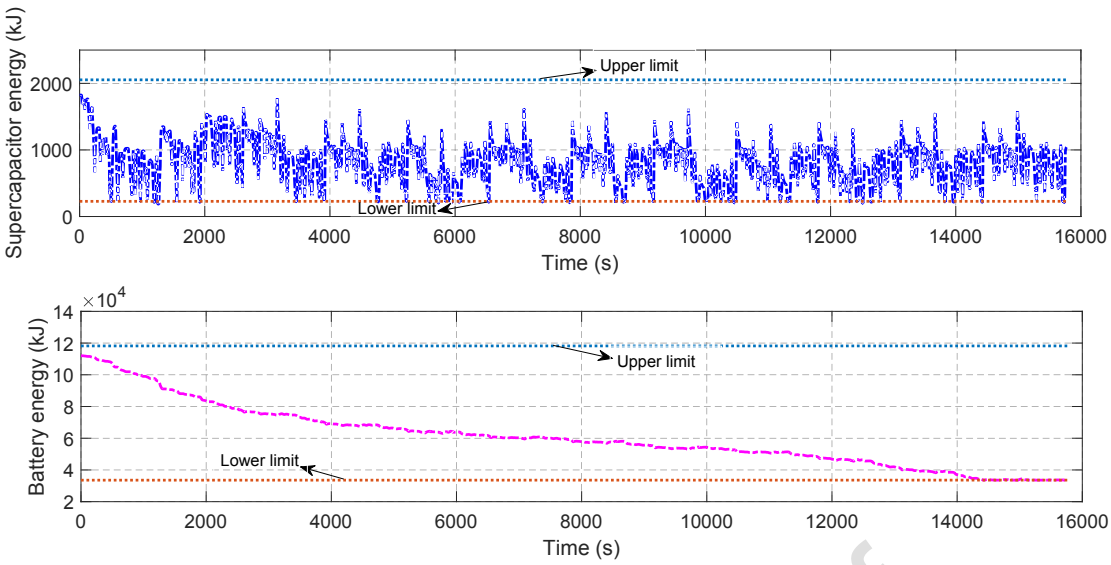

Fig.19 The remaining energy of the battery and the supercapacitor is obtained by power limits management module

Fig.20, (a), (b) and (c) are obtained based on global DP, V0.8-DP and adaptive power allocation, respectively. It is obvious that the maximum depth of battery charge and discharge cycles obtained by adaptive power allocation (shown in Fig.20(c)) is smaller than those obtained by global DP (shown in Fig.20(a)) and V0.8-DP (shown in Fig.20(b)). Also, the number of battery cycles with adaptive low-pass filtering is 126, which is decreased by 50.4% and 48.4% compared with those obtained by global DP and V0.8-DP, respectively. By using the rain flow cycle counting, the battery lifetime evaluations are compared between the two cases that PHEV with adaptive power allocation method and PHEB with dynamic programming based on the assumption that the PHEB fulfills 12 times of the CTUDC per day. The result shows that the battery service lifetime is improved from 776 days with the dynamic programming to 1102 days of the PHES with the adaptive power allocation resulting in 54.9% battery lifetime extension.

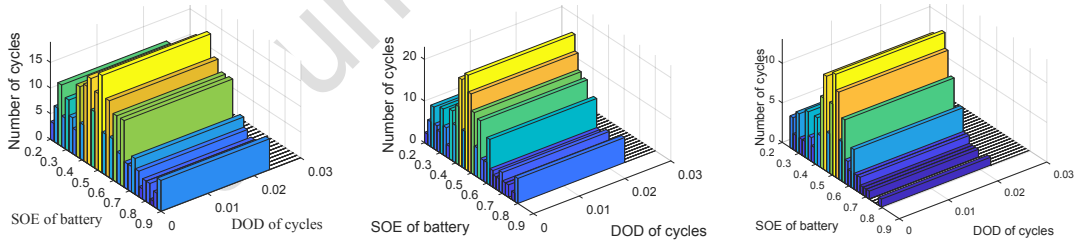

(a) Global DP (b) V0.8-DP (c) Adaptive power allocation

Fig.20 Number and depth of battery charge and discharge cycles

5.3 Life cycle cost analysis

According to the general design requirements, the PHEB has a life cycle of 12 years. This paper assumes that the PHEB runs twelve CTUDCs (about 4 hours in total) one day and works 300 days a year. The capacity of the battery pack is 60Ah, and the mass of the battery pack is 353kg (data from Yutong Bus). The management fee for a ton of aging lithium-ion batteries is $1,170, which includes a $1,120 collection cost and a $45 landfill dump fee [66]. The battery life is 776 days based on DP and battery life model, so the battery needs to be replaced four times, and the management cost of aged battery is $1652 based on Eq.23. The battery life is 809 days based on V0.8-DP and battery life model, so the battery needs to be replaced four times, and the management cost of aged battery is $1652 based

on Eq.23. The battery life is 1102 days based on DP and battery life model, so the battery needs to be replaced two times, and the management cost of aged battery is $826 based on Eq.23.

For powertrain configuration a, the battery aging cost is $13.37 per day under the global DP. The battery aging cost is $12.81 per day under the V0.8-DP. For the powertrain configuration b, the battery aging cost is $8.64 per day after adaptive power allocation, because the supercapacitor group is added.

Table.4 Comparison of life cycle cost under different configurations and different algorithms

Parameters	**Powertrain configuration a**		**Powertrain configuration b**
Algorithms	Global DP	V-DP	Adaptive power allocation
Battery pack cost ($)	48132	46116	31104
Battery service life (%)	100	104.3	154.9
Supercapacitor group cost ($)	0	0	2268
Fuel cost ($)	29354	30062	33892
Electricity cost ($)	11631	10977	11400
Aged batteries management cost ($)	1652	1652	826
Total cost ($)	90769	88807	79490
Total economy (%)	100	97.8	87.6

As shown in Table 3, the powertrain configuration a has the lowest equivalent fuel consumption based on the global DP with the highest battery aging cost. Compared to vehicle configuration a, configuration b has the initial cost of supercapacitor group with the reduced battery aging cost. Considering the battery aging cost, the initial installation cost of the supercapacitor group and the equivalent fuel consumption costs, the total cost of the vehicle configuration b under the adaptive power allocation is the lowest. Comparing to the powertrain configuration a under the global DP, the cost of the powertrain configuration a based on V0.8-DP is reduced by 2.2%. Compared with the configuration a under the global DP, the cost of the configuration b based on the adaptive power allocation is reduced by 12.4%. These data fully demonstrate that hierarchical optimization energy management strategy can suppress the battery aging greatly.

6. Conclusions:

This paper proposes a hierarchical optimization energy management strategy to suppress the battery aging for a PHEB with HESS. The PHEB simulation model is set up to run twelve CTUDCs. In the first-level, this paper proposes V-DP algorithm to allocate the power between ESS and engine, and the results show that when the threshold of SOC of ESS is 0.8, the total costs include battery aging cost, fuel consumption cost and electricity consumption cost are minimum. Compared with global DP, the battery service life is improved by 4.25% under V0.8-DP. In the second-level, firstly, this paper proposes adaptive low-pass filtering algorithm to distribute the power between supercapacitor and battery inside HESS, but the results show that supercapacitor appears severely over-discharged. Then, this paper proposes power limits management module to control the supercapacitor and battery working within the capacity range and redistribute the power between ESU and engine. The results show that compared with global DP, the battery service life is improved by 54.9% under power limits management module. In order to optimize the hierarchical optimization energy management strategy and analyze the life cycle economy, this paper proposes a simple but effective battery life quantification model based on rain-flow counting algorithm. The results show that compared with the global DP, the life cycle economy of the vehicle is improved by 2.2% and 12.4% under the V0.8-DP and adaptive power allocation respectively. In conclusion, the hierarchical optimization energy

management strategy can significantly inhibit battery aging and effectively improve the life cycle economy of the vehicle.

Acknowledgments

This work was supported by the Nature Science Foundation of China with Grant No. 51807008 and U1864202

Reference:

[1] M. Sedighizadeh, M. Esmaili, and N. Mohammadkhani, "Stochastic multi-objective energy management in residential microgrids with combined cooling, heating, and power units considering battery energy storage systems and plug-in hybrid electric vehicles," *Journal of Cleaner Production,* vol. 195, pp. 301-317, 2018/09/10/ 2018.

[2] L. Zhang, R. Long, C. Hong, and X. Huang, "Performance changes analysis of industrial enterprises under energy constraints," *Resources Conservation & Recycling,* vol. 136, pp. 248-256, 2018.

[3] J. Li, Q. Yang, H. Mu, S. Le Blond, and H. He, "A new fault detection and fault location method for multi-terminal high voltage direct current of offshore wind farm," *Applied Energy,* vol. 220, pp. 13-20, 2018/06/15/ 2018.

[4] Q. Yang, S. L. Blond, F. Liang, W. Yuan, M. Zhang, and J. Li, "Design and Application of Superconducting Fault Current Limiter in a Multiterminal HVDC System," *IEEE Transactions on Applied Superconductivity,* vol. 27, no. 4, pp. 1-5, 2017.

[5] H. Fathabadi, "Utilizing solar and wind energy in plug-in hybrid electric vehicles," *Energy Conversion & Management,* vol. 156, pp. 317-328, 2018.

[6] J. Li, M. Zhang, Q. Yang, Z. Zhang, and W. Yuan, "SMES/Battery Hybrid Energy Storage System for Electric Buses," *IEEE Transactions on Applied Superconductivity,* vol. 26, no. 4, pp. 1-5, 2016.

[7] J. Garcia, D. Millet, P. Tonnelier, S. Richet, and R. Chenouard, "A novel approach for global environmental performance evaluation of electric batteries for hybrid vehicles," *Journal of Cleaner Production,* vol. 156, pp. 406-417, 2017/07/10/ 2017.

[8] N. Denis, M. R. Dubois, J. P. F. Trovão, and A. Desrochers, "Power Split Strategy Optimization of a Plug-in Parallel Hybrid Electric Vehicle," *IEEE Transactions on Vehicular Technology,* vol. 67, no. 1, pp.

315-326, 2018.

[9] N. Rietmann and T. Lieven, "How policy measures succeeded to promote electric mobility – Worldwide review and outlook," *Journal of Cleaner Production,* vol. 206, pp. 66-75, 2019/01/01/ 2019.

[10] J. Garcia, D. Millet, and P. Tonnelier, "A tool to evaluate the impacts of an innovation on a product's recyclability rate by adopting a modular approach: automotive sector application," (in English), vol. 2015, no. 1, pp. 1-18, 2015 2015.

[11] S. Ebrahimi, R. Akbari, F. Tahami, and H. Oraee, "An Isolated Bidirectional Integrated Plug-in Hybrid Electric Vehicle Battery Charger with Resonant Converters," *Electric Power Components and Systems,* vol. 44, no. 12, pp. 1371-1383, 2016.

[12] C. Zhuge, B. Wei, C. Dong, C. Shao, and Y. Shan, "Exploring the future electric vehicle market and its impacts with an agent-based spatial integrated framework: A case study of Beijing, China," *Journal of Cleaner Production,* vol. 221, pp. 710-737, 2019/06/01/ 2019.

[13] M. Montazeri-Gh and M. Mahmoodi-K, "Optimized predictive energy management of plug-in hybrid electric vehicle based on traffic condition," *Journal of Cleaner Production,* vol. 139, pp. 935-948, 2016/12/15/ 2016.

[14] S. Xie, H. He, and J. Peng, "An energy management strategy based on stochastic model predictive control for plug-in hybrid electric buses," *Applied Energy,* vol. 196, pp. 279-288, 2017.

[15] S. Jung and H. Y. Jung, "Charge/discharge characteristics of Li‐ion batteries with two‐phase active materials: a comparative study of LiFePO4 and LiCoO2 cells," *International Journal of Energy Research,* vol. 40, no. 11, pp. 1541-1555, 2016.

[16] OMAR *et al.*, "Lithium iron phosphate based battery – Assessment of the aging parameters and development of cycle life model," *Applied Energy,* vol. 113, no. 1, pp. 1575-1585, 2014.

[17] L. X. Yuan, Z. H. Wang, W. X. Zhang, X. L. Hu, and J. B. Goodenough, "Development and challenges of LiFePO4 cathode material for lithium-ion batteries," *Energy & Environmental Science,* vol. 4, no. 2, pp. 269-0, 2010.

[18] H. Yuan, L. Hao, Y. C. Lu, Y. Hou, and L. Quan, "Electrophoretic lithium iron phosphate/reduced graphene oxide composite for lithium ion battery cathode application," *Journal of Power Sources,* vol. 284, pp. 236-244, 2015.

[19] J. Alves *et al.*, "Indirect methodologies to estimate energy use in vehicles: Application to battery electric vehicles," *Energy Conversion & Management,* vol. 124, pp. 116-129, 2016.

[20] J. Li *et al.*, "Analysis of a new design of the hybrid energy storage system used in the residential m-CHP systems," *Applied Energy,* vol. 187, pp. 169-179, 2017/02/01/ 2017.

[21] C. Jian and A. Emadi, "A New Battery/UltraCapacitor Hybrid Energy Storage System for Electric, Hybrid, and Plug-In Hybrid Electric Vehicles," *IEEE Transactions on Power Electronics,* vol. 27, no. 1, pp. 122-132, 2011.

[22] Q. Yang, S. Le Blond, R. Aggarwal, Y. Wang, and J. Li, "New ANN method for multi-terminal HVDC protection relaying," *Electric Power Systems Research,* vol. 148, pp. 192-201, 2017/07/01/ 2017.

[23] M. Sedighizadeh, G. Shaghaghi-shahr, M. Esmaili, and M. R. Aghamohammadi, "Optimal distribution feeder reconfiguration and generation scheduling for microgrid day-ahead operation in the presence of electric vehicles considering uncertainties," *Journal of Energy Storage,* vol. 21, pp. 58-71, 2019/02/01/ 2019.

[24] F. Barzegar, A. Bello, D. Momodu, M. J. Madito, J. Dangbegnon, and N. Manyala, "Preparation and characterization of porous carbon from expanded graphite for high energy density supercapacitor in aqueous electrolyte," *Journal of Power Sources,* vol. 309, pp. 245-253, 2016.

[25] J. Li, Q. Yang, F. Robinson, F. Liang, M. Zhang, and W. Yuan, "Design and test of a new droop control algorithm for a SMES/battery hybrid energy storage system," *Energy,* vol. 118, pp. 1110-1122, 2017/01/01/ 2017.

[26] A. Mayyas, M. Omar, M. Hayajneh, and A. R. Mayyas, "Vehicle's lightweight design vs. electrification from life cycle assessment perspective," *Journal of Cleaner Production,* vol. 167, pp. 687-701, 2017/11/20/ 2017.

[27] B. Sen, N. C. Onat, M. Kucukvar, and O. Tatari, "Material footprint of electric vehicles: A multiregional life cycle assessment," *Journal of Cleaner Production,* vol. 209, pp. 1033-1043, 2019/02/01/ 2019.

[28] KOOHIKAMALI, RAHIM, A. N., and MOKHLIS, "Smart power management algorithm in microgrid consisting of photovoltaic, diesel, and battery storage plants considering variations in sunlight, temperature, and load," *Energy Conversion & Management,* vol. 84, pp. 562-582, 2014.

[29] D. Pavković, M. Lobrović, M. Hrgetić, and A. Komljenović, "A Design of Cascade Control System and Adaptive Load Compensator for Battery/Ultracapacitor Hybrid Energy Storage-based Direct Current Microgrid," *Energy Conversion & Management,* vol. 114, pp. 154-167, 2016.

[30] J. Li, R. Xiong, Q. Yang, F. Liang, M. Zhang, and W. Yuan, "Design/test of a hybrid energy storage system for primary frequency control using a dynamic droop method in an isolated microgrid power system," *Applied Energy,* vol. 201, pp. 257-269, 2017/09/01/ 2017.

[31] Z. Song, J. Li, J. Hou, H. Hofmann, M. Ouyang, and J. Du, "The Battery-Supercapacitor Hybrid Energy Storage System in Electric Vehicle Applications: A Case Study," *Energy,* vol. 154, 2018.

[32] F. Abnisa and M. A. W. D. Wan, "A review on co-pyrolysis of biomass: An optional technique to obtain a high-grade pyrolysis oil," *Energy Conversion & Management,* vol. 87, pp. 71-85, 2014.

[33] M. A. Hannan, F. A. Azidin, and A. Mohamed, "Multi-sources model and control algorithm of an energy

management system for light electric vehicles," *Energy Conversion & Management,* vol. 62, no. 5, pp. 123-130, 2012.

[34] C. Zheng, G. Xu, K. Xu, Z. Pan, and L. Quan, "An energy management approach of hybrid vehicles using traffic preview information for energy saving," *Energy Conversion & Management,* vol. 105, pp. 462-470, 2015.

[35] H.-S. Lee, J.-S. Kim, Y.-I. Park, and S.-W. Cha, "Rule-based power distribution in the power train of a parallel hybrid tractor for fuel savings," *International Journal of Precision Engineering and Manufacturing-Green Technology,* vol. 3, no. 3, pp. 231-237, 2016/07/01 2016.

[36] Y. Li, K. Xie, L. Wang, and Y. Xiang, "The impact of PHEVs charging and network topology optimization on bulk power system reliability," *Electric Power Systems Research,* vol. 163, pp. 85-97, 2018.

[37] S. Ahmadi, S. M. T. Bathaee, and A. H. Hosseinpour, "Improving fuel economy and performance of a fuel-cell hybrid electric vehicle (fuel-cell, battery, and ultra-capacitor) using optimized energy management strategy," *Energy Conversion & Management,* vol. 160, pp. 74-84, 2018.

[38] Y. Li, X. Huang, D. Liu, M. Wang, and J. Xu, "Hybrid energy storage system and energy distribution strategy for four-wheel independent-drive electric vehicles," *Journal of Cleaner Production,* vol. 220, pp. 756-770, 2019/05/20/ 2019.

[39] W. Zhen, J. Xu, and D. Halim, "HEV power management control strategy for urban driving," *Applied Energy,* vol. 194, pp. 705-714, 2017.

[40] M. Sedighizadeh, M. Dakhem, M. Sarvi, and H. H. Kordkheili, "Optimal reconfiguration and capacitor placement for power loss reduction of distribution system using improved binary particle swarm optimization," *International Journal of Energy and Environmental Engineering,* vol. 5, no. 1, p. 3, 2014/01/02 2014.

[41] P. Shen, J. Li, X. Zhan, and Z. Zhao, "Particle swarm optimization of driving torque demand decision based on fuel economy for plug-in hybrid electric vehicle," *Energy,* vol. 123, pp. 89-107, 2017.

[42] H. Hemi, J. Ghouili, and A. Cheriti, "A real time fuzzy logic power management strategy for a fuel cell vehicle," *Energy Conversion & Management,* vol. 80, no. 4, pp. 63-70, 2014.

[43] X. Wang, H. He, F. Sun, and J. Zhang, "Application Study on the Dynamic Programming Algorithm for Energy Management of Plug-in Hybrid Electric Vehicles," *Energies,* vol. 8, no. 4, pp. 3225-3244, 2015.

[44] J. Li, A. M. Gee, Z. Min, and W. Yuan, "Analysis of battery lifetime extension in a SMES-battery hybrid energy storage system using a novel battery lifetime model," *Energy,* vol. 86, pp. 175-185, 2015.

[45] S. Kotra and M. K. Mishra, "A Supervisory Power Management System for a Hybrid Microgrid with HESS," *IEEE Transactions on Industrial Electronics,* vol. PP, no. 99, pp. 1-1, 2017.

[46] B. Wang, J. Xu, B. Cao, and X. Zhou, "A novel multimode hybrid energy storage system and its energy management strategy for electric vehicles," *Journal of Power Sources,* vol. 281, pp. 432-443, 2015.

[47] X. Shi, A. Dini, Z. Shao, N. H. Jabarullah, and Z. liu, "Impacts of photovoltaic/wind turbine/microgrid turbine and energy storage system for bidding model in power system," *Journal of Cleaner Production,* 2019/04/15/ 2019.

[48] L. Liang, Y. Zhang, Y. Chao, B. Yan, and C. M. Martinez, "Model predictive control-based efficient energy recovery control strategy for regenerative braking system of hybrid electric bus," *Energy Conversion & Management,* vol. 111, pp. 299-314, 2016.

[49] S. Berrazouane and K. Mohammedi, "Parameter optimization via cuckoo optimization algorithm of fuzzy controller for energy management of a hybrid power system," *Energy Conversion & Management,* vol. 78, no. 1, pp. 652-660, 2014.

[50] L. Yi, S. Lin, and G. Tu, "Optimal sizing and control strategy of isolated grid with wind power and energy

storage system," *Energy Conversion & Management,* vol. 80, no. 4, pp. 407-415, 2014.

[51] C. L. Nguyen and H. H. Lee, "Power Management Approach to Minimize Battery Capacity in Wind Energy Conversion Systems," *IEEE Transactions on Industry Applications,* vol. PP, no. 99, pp. 1-1, 2017.

[52] L. W. Chong, Y. W. Wong, R. K. Rajkumar, and D. Isa, "An optimal control strategy for standalone PV system with Battery-Supercapacitor Hybrid Energy Storage System," *Journal of Power Sources,* vol. 331, pp. 553-565, 2016.

[53] M. Qiang, X. Lei, H. Cui, L. Wei, and M. Pecht, "Remaining useful life prediction of lithium-ion battery with unscented particle filter technique," *Microelectronics Reliability,* vol. 53, no. 6, pp. 805-810, 2013.

[54] J. Du, Z. Liu, Y. Wang, and C. Wen, "A fuzzy logic-based model for Li-ion battery with SOC and temperature effect," in *IEEE International Conference on Control & Automation*, 2014.

[55] J. Li *et al.*, "Design and real-time test of a hybrid energy storage system in the microgrid with the benefit of improving the battery lifetime," *Applied Energy,* vol. 218, pp. 470-478, 2018.

[56] S. Li, H. He, and J. Li, "Big data driven lithium-ion battery modeling method based on SDAE-ELM algorithm and data pre-processing technology," *Applied Energy,* vol. 242, pp. 1259-1273, 2019.

[57] G. Li, J. Zhang, and H. He, "Battery SOC constraint comparison for predictive energy management of plug-in hybrid electric bus," *Applied Energy,* vol. 194, 2016.

[58] X. Wang, H. He, F. Sun, X. Sun, and H. Tang, "Comparative Study on Different Energy Management Strategies for Plug-In Hybrid Electric Vehicles," *Energies,* vol. 6, no. 11, pp. 5656-5675, 2013.

[59] J. Peng, H. He, and X. Rui, "Rule based energy management strategy for a series–parallel plug-in hybrid electric bus optimized by dynamic programming," *Applied Energy,* vol. 185, 2016.

[60] J. Du *et al.*, "Battery degradation minimization oriented energy management strategy for plug-in hybrid

electric bus with multi-energy storage system," *Energy*.

[61] Z. Song *et al.*, "Multi-objective optimization of a semi-active battery/supercapacitor energy storage system for electric vehicles," *Applied Energy,* vol. 135, pp. 212-224, 2014.

[62] J. Peng, H. He, and R. Xiong, "Rule based energy management strategy for a series–parallel plug-in hybrid electric bus optimized by dynamic programming," *Applied Energy,* vol. 185, pp. 1633-1643, 2017.

[63] S. Zhang and X. Rui, "Adaptive energy management of a plug-in hybrid electric vehicle based on driving pattern recognition and dynamic programming," *Applied Energy,* vol. 155, pp. 68-78, 2015.

[64] A. Niesłony, "Determination of fragments of multiaxial service loading strongly influencing the fatigue of machine components," *Mechanical Systems & Signal Processing,* vol. 23, no. 8, pp. 2712-2721, 2009.

[65] C. Ju, W. Peng, L. Goel, and X. Yan, "A Two-layer Energy Management System for Microgrids with Hybrid Energy Storage considering Degradation Costs," *IEEE Transactions on Smart Grid,* vol. PP, no. 99, pp. 1-1, 2017.

[66] W. Xue, G. Gaustad, C. W. Babbitt, and K. Richa, "Economies of scale for future lithium-ion battery recycling infrastructure," *Resources Conservation & Recycling,* vol. 83, no. 1, pp. 53-62, 2014.

Highlights:

1. A method are proposed to improve fuel economy while suppressing battery aging
2. Numbers of battery charge and discharge cycles are reduced based on the algorithm
3. Adaptive power allocation algorithm could reduce battery charge and discharge rate
4. A life model is developed for quantitative analysis of battery lifetime improvement